Batteries & Supercaps

Research Article
doi.org/10.1002/batt.202100399

Chemistry
Europe
European Chemical
Societies Publishing

www.batteries-supercaps.org

A Combined Lithium Intercalation and Plating Mechanism Using Conductive Carbon-Fiber Electrodes

Tommy Zijian Zhao,[a] Wesley M. Dose,[a] and Michael F. L. De Volder*[a]

Lithium-metal anodes (LMAs) are desirable for next-generation rechargeable batteries because of their high energy density. However, in practical applications they are hindered by inhomogeneous and uncontrolled lithium-dendrite deposition during cycling. Herein, we propose a dual charge storage mechanism, using freestanding carbon-fiber paper (CFP) with carbon fillers electrode. These CFP electrodes are manufactured at an industrial scale and act both as a host for lithium (Li) intercalation and as a conductive and porous 3D scaffold for Li plating/stripping. The CFP electrode exhibits excellent long-term cycling stability, as evidenced by Coulombic efficiencies of over 99.5% on the 250th cycle in CFP│Li half-cells with a lithiation capacity of 1.5 mA h cm^{-2} and current density of 0.5 mA cm^{-2}. We also demonstrate that the CFPs are sufficiently electrically conductive to operate in small pouch cells without metal foil current collectors, further improving the energy density of the proposed electrodes.

Introduction

The ever-growing energy demand from modern portable electronics, power tools and electric vehicles calls for a matching development in lithium-ion batteries (LIBs) that offer high power density, energy density, and long cycle life.[1] Despite numerous improvements to the performance of LIBs over the past years, commercial LIB electrode materials (e.g., graphite anodes, capacity of 372 mA h g^{-1}) are struggling to keep up with the demands from emerging applications.[2–5] Lithium-metal anodes (LMAs) are promising for next-generation rechargeable batteries due to their ultra-high specific capacity ($\sim$3860 mA h g^{-1}) and low negative reduction potential (-3.040 V vs. standard hydrogen electrode).[6–8] By pairing LMAs with appropriate cathodes, the resulting lithium-metal batteries may therefore achieve much higher theoretical energy densities than commercial LIBs.[9,10] However, LMAs suffer from several critical issues that are intrinsically caused by the inhomogeneous and poorly controlled lithium (Li) plating process during cycling, which limits their practical applications. The large volume expansion of LMAs leads to repeated fracture and reformation of the solid electrolyte interphase (SEI), which continuously consumes active Li ions and creates electronically isolated Li as the dendrites break apart from the electrode during delithiation, resulting in low Coulombic efficiency (CE) and short cycle-life.[6] Furthermore, Li tends to plate in the form of dendrites that can pierce through the separator, leading to internal short-circuiting and thermal runaway.[11,12]

To balance the opportunities and challenges offered by classic intercalation anodes and LMAs, we propose a free-standing graphitized carbon fiber paper (CFP) with carbon fillers as an anode that combines the two energy storage mechanisms. These new anodes are advantageous because i) both the graphitic fibers and fillers are able to store considerable energy by intercalation ($>$1.0 mA h cm^{-2}); ii) we show that these electrodes require no additional coating to achieve stable Li plating/stripping with low nucleation overpotential; iii) CFP is highly conductive and can therefore operate without metal current collectors; and iv) processes have been established to manufacture and modify CFP cost-effectively at large scale.[13,14] We show that these electrodes can operate in a stable two-step lithiation/delithiation process, where Li ions firstly intercalate into the graphitic carbon fibers and then plate on the carbon fibers as depicted in Figure 1(a).

In this work, we build on two previously reported strategies to improve the stability of LMAs: i) modification of liquid electrolytes using alternative lithium salts and additives such as Lithium bis(trifluoromethanesulfonyl)imide (LiTFSI),[15,16] lithium bis(fluorosulfonyl)imide (LiFSI),[17,18] Lithium bis(oxalato)borate (LiBOB),[19] Lithum Nitrate (LiNO$_3$)[20–24] to improve the reversibility of LMAs by a range of effects including the formation of a more stable SEI and the suppression of Li dendrite growth,[25,26] ii) using porous 3D host structures with high surface area to reduce local current density, thus promoting smooth Li deposition on the hosts and reducing Li dendrite growth (based on Sand's diffusion model).[27–29] Carbon in various forms has been a popular choice to create conductive scaffolds for Li plating and stripping in LMAs. These structures include graphite particles,[30] graphene sponges,[31–33] carbon nanospheres,[34] carbon modified Ni foams,[35] carbon nanotube (CNT) paper[36,37] and composites,[38,39] and modified or doped carbon-fiber networks.[40–48] CEs of up to $\sim$99% for 200–300 cycles in a half-cell configuration (Li metal as the counter electrode) have been

[a] T. Zijian Zhao, Dr. W. M. Dose, Prof. M. F. L. De Volder
Institute for Manufacturing
University of Cambridge
Cambridge, CB3 0FS, United Kingdom
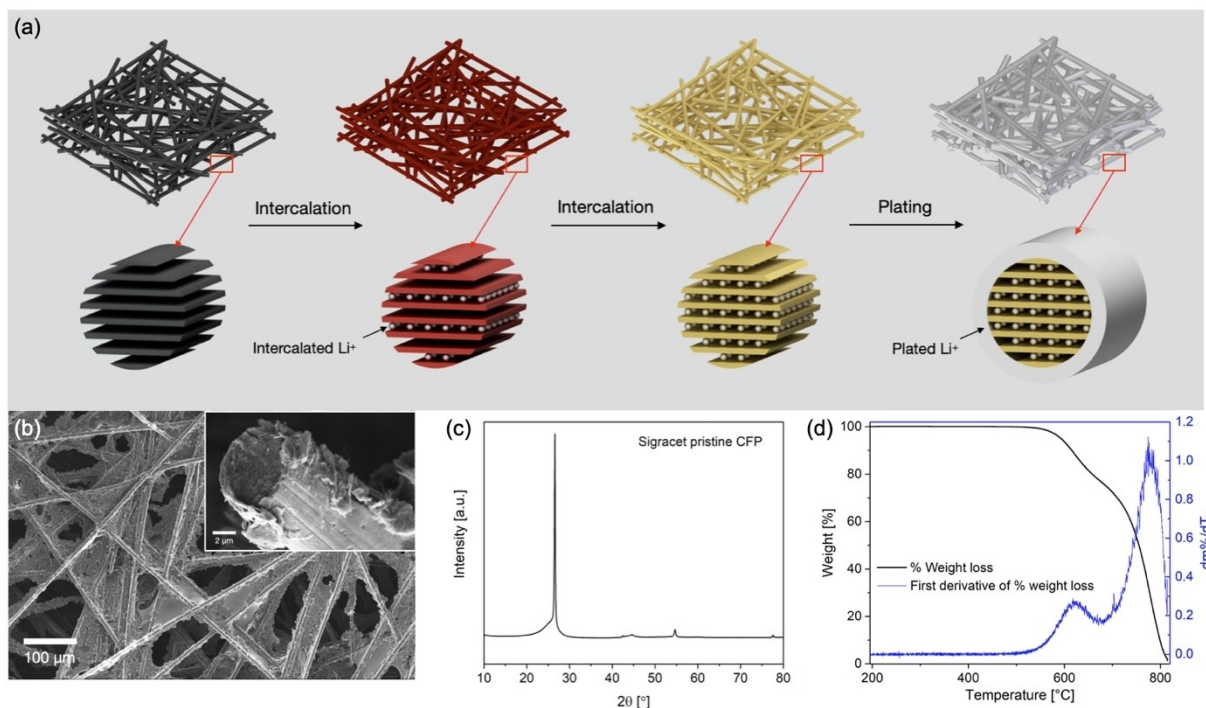E-mail: mfld2@cam.ac.uk

Figure 1. a) Schematic diagrams of the two-step Li intercalation and plating process on the CFP electrode. b) SEM images of CFP; inset shows the cross-section of a carbon fiber. c) X-ray diffraction pattern of the CFP. d) Thermogravimetric analysis mass loss and differential mass loss profiles of the CFP.

reported using these matrices.[49] However, manufacturing challenges, as well as issues with the weight and volume of the LMA scaffolds are typically not discussed in any depth. To alleviate these challenges, recent work on LMAs suggests exploiting the intercalation of Li ions into graphitic carbon fibers or particles, which simultaneously generates lithiophilic Li intercalation compounds that ensures efficient Li plating,[30,50] and can provide additional energy storage which leads to improved energy density.[51] As a result, an impressive areal capacity of up to 8 mAh cm^{-2} was obtained,[50,51] but with limited CEs of only up to 98% on the 50th cycle, and very low volumetric capacities (electrodes of 1 to 10 mm thick). In this work, we present anodes with a dual intercalation – plating charge storage mechanism that achieve higher CEs of over 99.5% on the 250th cycle and 99% on the 300th cycle in CFP|Li half-cells, with low nucleation overpotentials of ca. −6 mV. These are among the best CE versus cycle values reported so far for LMAs with a lithiation capacity of more than 1.5 mAh cm^{-2}. In addition, the fabrication process of the electrodes presented in this work is scalable and the surface area of the proposed electrodes is low, which leads to high Coulombic efficiencies in the initial cycles. The capacity retention of the intercalation contribution on each cycle is studied independently to reveal both the energy storage and the degradation mechanism of the CFP electrode. This process is underpinned using an *operando* microscopic imaging technique with optical battery cells.

Results and Discussion

Scanning electron microscope (SEM) images of a pristine CFP electrode are shown in Figure 1(b). It mainly consists of carbon fibers with diameters of ca. 7–9 μm that are held together by rough graphitic carbon fillers. The structure used in this study has a porosity of ca. 90% when uncompressed (calculation shown in the supplementary information) and a compressibility of ca. 33% (at 1 MPa).[13] The CFP is anisotropic as the carbon fibers have favored in-plane orientations, and therefore their properties such as permeability, thermal conductivity and diffusivity differ between the in-plane and through-plane directions.[52–54] An X-ray diffraction (XRD) pattern of the CFP is shown in Figure 1(c). The diffraction peaks of graphite (002) at $2\theta = 26.5°$, (004) at $2\theta = 54.6°$, can be identified, as well as two smaller peaks at around $2\theta = 42°$, (100) & (101) and $2\theta = 78°$, (110). As shown in Figure 1(d), thermogravimetric analysis (TGA) results indicate that the combustion reaction of the CFP in air occurs at close to 600 °C and finishes at above 800 °C, which is the same range as graphite.[55] The weight loss curve shows two stages which is also apparent in the two peaks of the weight first derivative curve.

Our proposed two-step lithiation/delithiation mechanism on CFP is illustrated in Figure 1(a). Firstly, the graphitic carbon acts as an intercalation host that Li ions gradually occupy. As the full intercalation capacity is reached, the potential drops below 0 V (all potentials quoted in this work are versus Li/Li$^+$), and Li starts to plate on the surfaces of the conductive carbon fiber network and extend in between the pores. Figure 2 reveals this process using optical images taken from an
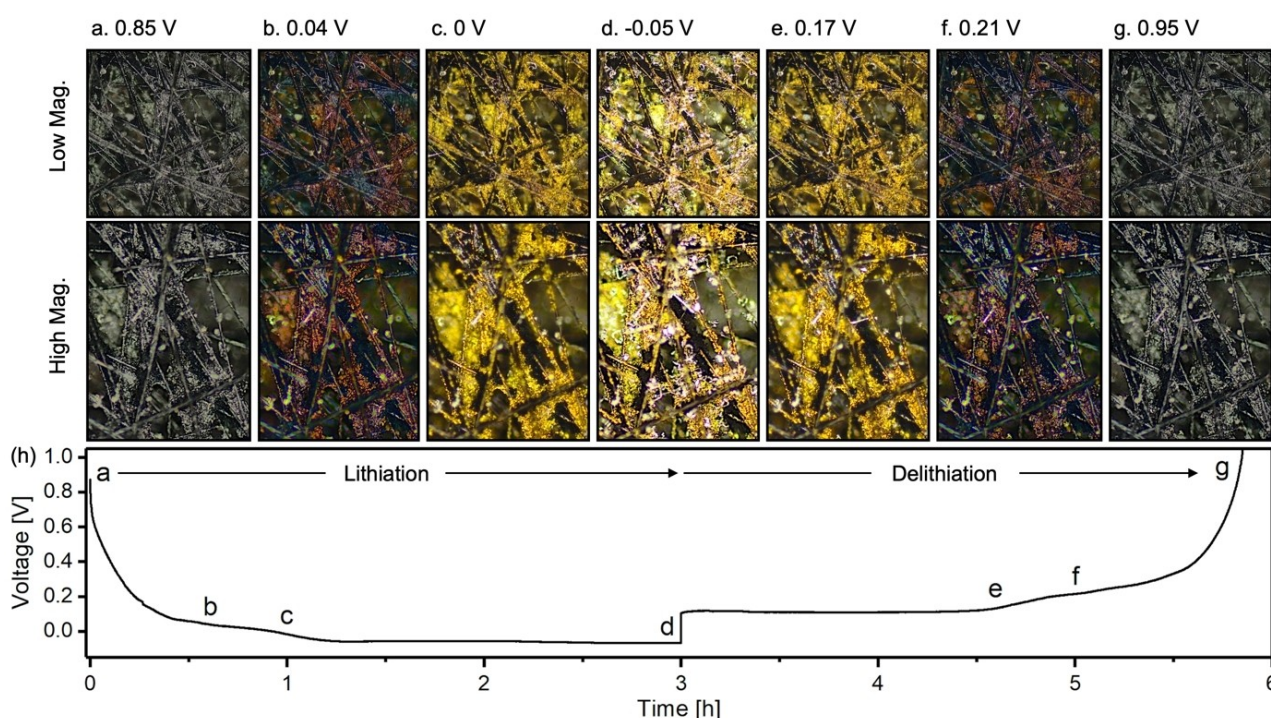
Batteries & Supercaps

Research Article
doi.org/10.1002/batt.202100399

Chemistry Europe
European Chemical
Societies Publishing

Figure 2. a–g) Morphology evolution of a CFP electrode during a two-step lithiation/delithiation process (intercalation and plating), observed in-situ with an optical battery cell. h) Galvanostatic lithiation/delithiation profile of the CFP|Li optical cell at a current density of 1.0 mA cm^{-2}.

operating battery cell when 3.0 mA h cm^{-2} of capacity is deposited and stripped at a current density of 1.0 mA cm^{-2}. Figure 2(a–c) shows the color of the CFP changing from grey to reddish brown then to gold, as a result of an increasing amount of Li being intercalated into the graphitic carbon in agreement with literature.[56] This is confirmed by the voltage plateaus shown in Figure 2(h) between point *a* and *c*, which correspond to the formation of various intercalation compounds (LiC$_{72}$, LiC$_{36}$, LiC$_{27}$, LiC$_{18}$, LiC$_{12}$ and LiC$_6$) as the potential approaches 0 V and intercalation progresses.[57,58] A dark blue/black color as shown in Figure S1(b) correlates to intercalation compounds with the lowest Li content, whereas the golden color correlates to the highest, which is the stage 1 LiC$_6$.[56] As the electrode is lithiated further, Li metal starts to nucleate and grow on the carbon fibers (see silver-colored deposits in Figure 2d) with a stable potential as shown in Figure 2(h) between point *c* and *d*. The porous and conductive structure offers abundant and well-distributed sites for Li nucleation, and ample room between the carbon fibers, allowing Li metal to grow in all directions instead of congregating as blocks as it has been shown to on planar Cu electrodes.[32] The above process reverses on the stripping half-cycle: first, Li metal around the carbon fibers is stripped (between point *d* and *e* in Figure 2h), as shown in Figure 2(e); intercalated Li ions are then removed as the cell potential approaches 1 V (between point *e* and *g* in Figure 2h), changing the color of the CFP from gold back to grey as shown in Figure 2(e–g). The CFP has no visible volume change during the lithiation/delithiation process due to the porous structure which helps accommodate the plated Li.

The amount of Li deposited and stripped in a cycle as calculated from the charge passed is used to evaluate the performance of the CFP electrode as an LMA. Figure S2 shows the 20th cycle of a CFP|Li cell with 3.0 mA h cm^{-2} of capacity deposited per cycle at a current density of 0.5 mA h cm^{-2}. A capacity of 1.227 mA h cm^{-2} is delivered via an intercalation mechanism (calculated as the capacity delivered before the voltage reaches 0 V) and 1.773 mA h cm^{-2} by plating (40.9% and 59.1% of the overall lithiation capacity respectively), with a CE of 99.5% and a low Li nucleation overpotential of only ca. −6 mV.[34,59]

Uniquely, the highly conductive CFP electrode circumvents the requirement for an additional Cu current collector, as proven by the stable performance of a CFP|Li pouch cell with a freestanding CFP electrode as shown in Figure S3 (more details later). The CFP electrode thus has a practical reversible gravimetric specific capacity of 746 mA h g^{-1} (based on 3 mA h cm^{-2} of lithiation capacity and the areal weight of the above CFP electrode of 4.03 mg cm^{-2}), which is more than 3 times higher than that of commercial graphite electrode (ca. 244 mA h g^{-1}) if the weight of the Cu current collector is taken into account, assuming natural graphite (360 mA h g^{-1}) with a mass loading of 7.5 mg cm^{-2} coated on each side of an 8 μm thick Cu current collector (calculation shown in supplementary information).

The efficiency and stability of the lithiation/delithiation process on CFP electrodes are demonstrated by long-term electrochemical tests with 1.5–2.0 mA h cm^{-2} of lithiation capacity per cycle at current densities of 0.5–1 mA cm^{-2} in half-cells. Figure 3(a) shows the CEs of lithiation/delithiation on CFP

Batteries & Supercaps

Research Article
doi.org/10.1002/batt.202100399

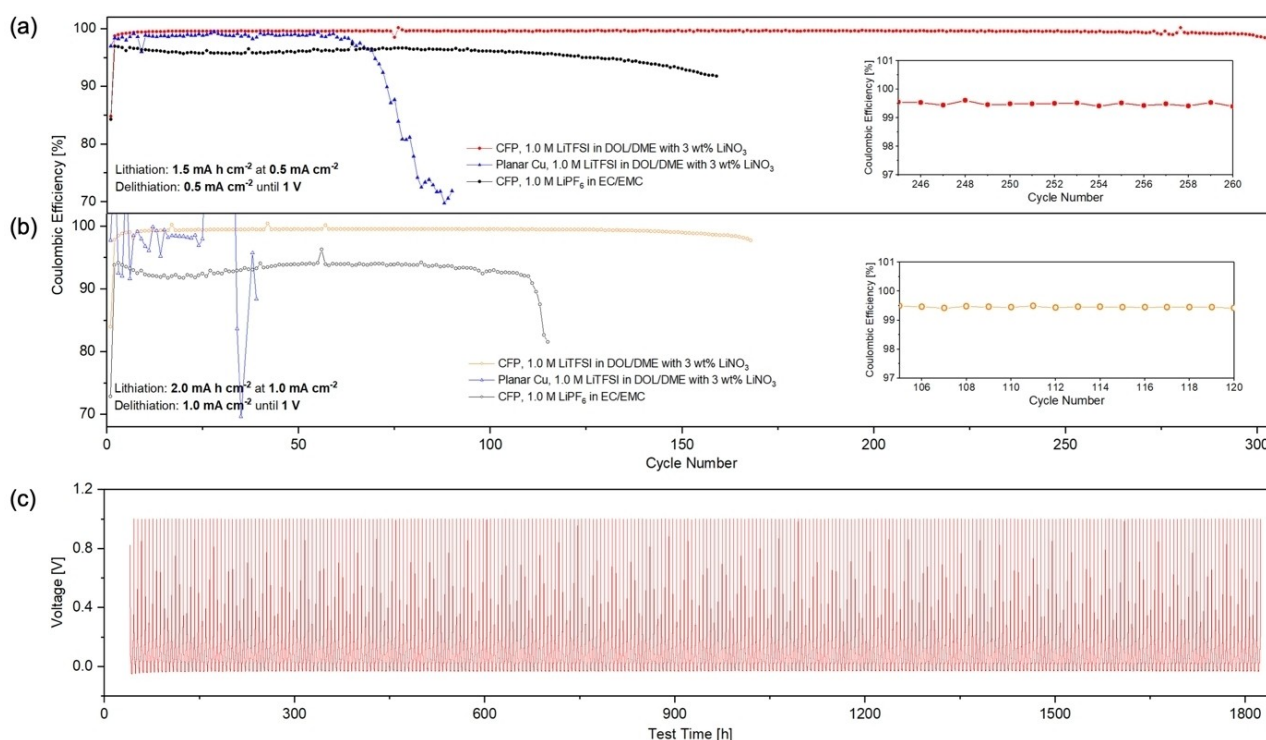**Chemistry Europe**
European Chemical
Societies Publishing

Figure 3. a and b) Coulombic efficiencies of lithiation/delithiation on CFP electrodes compared to that on planar Cu current collectors, with 1.0 M LiTFSI in DOL/DME with 3 wt% LiNO$_3$ electrolyte or 1.0 M LiPF$_6$ in EC/EMC electrolyte. The lithiation capacity is a) 1.5 mA h cm^{-2} per cycle at a current density of 0.5 mA cm^{-2}, and b) 2.0 mA h cm^{-2} per cycle at 1.0 mA cm^{-2}. Insets show the CE a) between cycle 245 and 260 and b) between cycle 105 and 120. c) Voltage vs. time profiles of all cycles for the CFP|Li cell with 1.0 M LiTFSI in DOL/DME with LiNO$_3$ electrolyte shown in (a).

as compared to that on planar Cu electrodes (lithiation capacity of 1.5 mA h cm^{-2} per cycle, current density of 0.5 mA cm^{-2}, 1.0 M LiTFSI in 1,3-dioxolane/1,2-dimethoxyethane (DOL/DME) with 3 wt% LiNO$_3$ electrolyte). The CE for the planar Cu electrode increases from 97.0% on the first cycle to 99.0% on the 7th cycle and remains at ca. 99% until the 60th cycle. As show in Figure 4(a), the voltage vs. specific capacity profiles of the lithiation/delithiation process on Cu (e.g., 2nd cycle) shows an evident voltage dip at the beginning of Li plating, followed by a flat voltage plateau. The difference between the lowest point of the voltage dip and the plateau is calculated as the Li metal nucleation potential,[60,61] which is −21.7 mV here. This value is mostly affected by the substrate as it signifies the energy barrier for metallic Li to deposit on the surface of the heterogenous electrode (Cu in this case). Meanwhile, the plateau overpotential on the cycle is ca. −28 mV and is mainly determined by the current density and the resistance to Li ion transfer.[61] As shown in Figure 4(b and c), from cycle 2 to 60, the nucleation potential on Cu substrate fluctuates between −20 and −60 mV and shows an increasing trend, which is propitious to the increasingly non-uniform Li nucleation; the plateau overpotential shows a gradual decrease to ca. −15 mV and maintains this value. During this process, as host-less dendritic Li forms and grows, the SEI continues to fracture and reform on the increased fresh Li surface area, causing larger amounts of Li to be trapped and some Li dendrites eventually breaking off from the islands and losing electrical contact with the electrode.[62] As a result, the CE decays rapidly from the 60th

cycle to below 75% on the 80th cycle. This is accompanied by a swift increase in plateau overpotential, because Li ions now have to diffuse through the increasingly porous and thick SEI layer to reach the nucleation sites, as well as a decrease in nucleation overpotential, since the additional Li now mostly deposits on the large amounts of unretrieved Li, which has a lower plating energy barrier and is more favorable than nucleation on Cu.[61]

In contrast, the first cycle CE for the CFP electrode is 85%. This value is reported without a 'pre-forming SEI step', whereby the working electrode is cycled at a low current density (such as 0.05 mA cm^{-2}) for a number of cycles before the electrochemical tests, as commonly included in other LMA studies to artificially improve the reported CE.[49] The CE then surpasses 99% after 3 cycles and remains above 99.5% for over 250 cycles, before slowly fading to 99% at the 300th cycle. The lower first cycle CE of the CFP electrode (as compared to Cu) is likely a result of its larger surface area, which leads to more Li being trapped to form the initial SEI layer. However, the unique conductive and porous 3D structure of the CFP electrode then allows Li to intercalate, plate and strip efficiently and repeatably, leading to the stable CE and voltage profiles as shown in Figure 3(a and c). Furthermore, as shown in Figure 4(a and b), the voltage vs. specific capacity profiles of the lithiation/delithiation process on CFP show no obvious dip at the beginning of Li plating stage, leading to very low and stable nucleation overpotentials of only ca. −5 mV for the first 210 cycles, and −6 to −7 mV for the next 100 cycles. These values
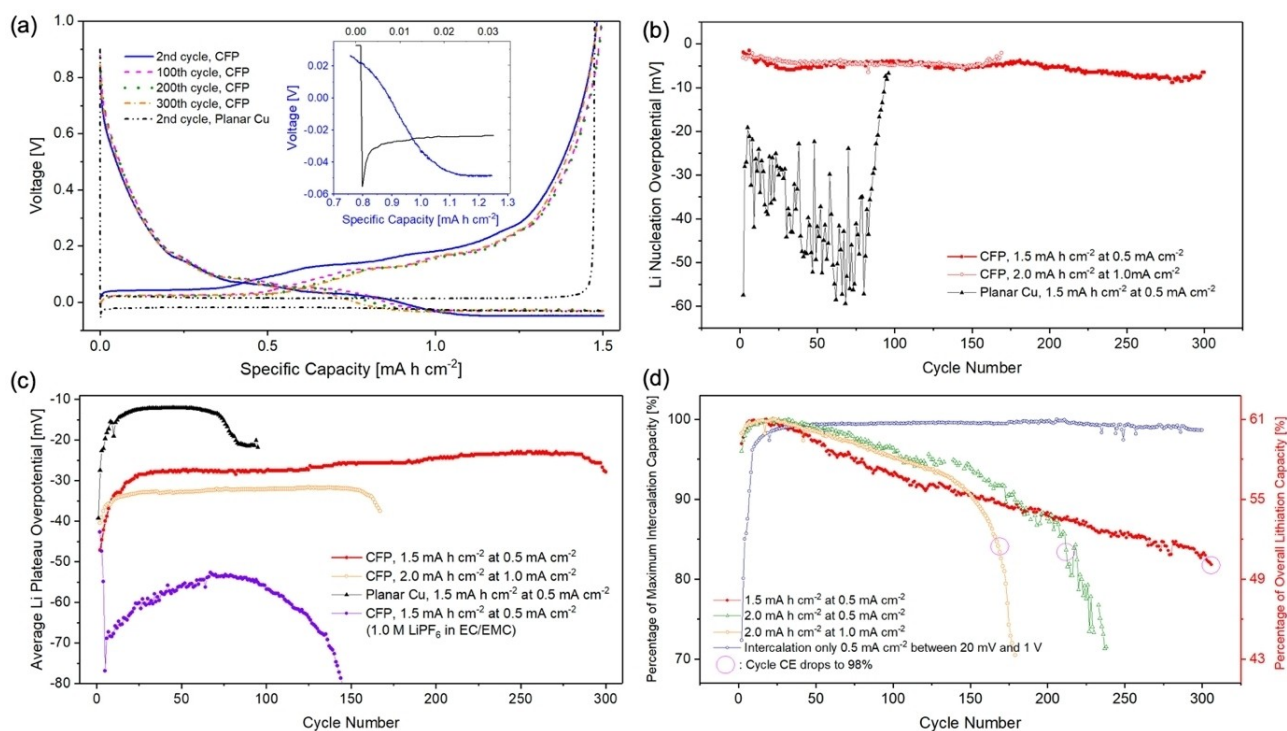
Figure 4. a) Voltage vs. specific capacity profiles of the 2nd, 100th, 200th and 300th cycles of the CFP|Li cell, and the 2nd cycle of the Cu|Li cell, with 1.0 M LiTFSI in DOL/DME with 3 wt% $LiNO_3$ electrolyte, with a lithiation capacity of 1.5 mA h cm^{-2} per cycle at a current density of 0.5 mA cm^{-2}. b) Li-nucleation overpotentials on each cycle for the 2 cells shown in (a), and the CFP|Li cell with a lithiation capacity of 2.0 mA h cm^{-2} per cycle at a current density of 1.0 mA cm^{-2}. c) Average Li plateau overpotentials on each cycle for the 3 cells shown in (b), and the CFP|Li cell with 1.0 M $LiPF_6$ in EC/EMC electrolyte. d) For 3 CFP|Li cells tested with current densities of 0.5, 0.5, 1.0 mA cm^{-2}, and lithiation capacities of 1.5, 2.0, 2.0 mA h cm^{-2}, respectively, the intercalation capacities of each deposition half-cycle as a percentage of the maximum intercalation capacity recorded for the cell; as well as for the cell with 0.5 mA cm^{-2} and 1.5 mA h cm^{-2}, the intercalation capacity as a percentage of the overall lithiation capacity. The intercalation capacities of a CFP electrode when cycled under a single stage intercalation protocol (between 20 mV and 1 V at a current density of 0.5 mA cm^{-2}) are shown as a comparison.

are an order of magnitude lower than that of the Cu substrate, due to the higher lithiophilicity and thus lower Li nucleation energy barrier of the Li-intercalated graphitic carbon of CFP compared to Cu.[50] As shown in Figure 4(c), the average plateau overpotentials on the CFP electrode are less than −30 mV for the majority of the 300 cycles and generally show a decreasing trend, which further proves the stability of the lithiation/ delithiation process for CFP. The electrochemical performance of the CFP electrode is still superior even when compared to that on planar Cu electrode with only 0.5 mA h cm^{-2} of lithiation capacity per cycle (less than the plating contribution of the CFP electrode on any cycle), at a current density of 0.5 mA cm^{-2}. As shown in Figure S4, the CE for the Cu electrode remains below 99% for 110 cycles and drops sharply to around 85%, with fluctuating nucleation overpotentials of up to −40 mV.

Figure 4(d) plots the lithiation capacity retention of the intercalation contribution (i.e., the capacity before the 0 V crossover) of the CFP electrode tested at various lithiation capacities and current densities. The intercalation contributions all reach their maximum after an activation process in the first ca. 20 cycles, then slowly decay in a linear fashion. With a lithiation capacity of 1.5 mA h cm^{-2} at 0.5 mA cm^{-2}, the inter-calation contribution reaches a maximum of ca. 60% of the overall cycle lithiation capacity on the 18th cycle. On the 300th cycle, the intercalation contribution is 83% of its maximum

value and ca. 50% of the total lithiation capacity on the cycle. In comparison, the CFP electrode shows a capacity loss of only 1.3% over 300 cycles when used as an intercalating electrode with no Li plating (at 0.5 mA cm^{-2}), as shown in Figure 4(d). Nevertheless, the overall cycle capacity and CE of the lithiation/ delithiation process on CFP remain unaffected by the decay of intercalation contribution, since the missing intercalation capacities are compensated by increasing amounts of Li plating/stripping that occur at a similarly high efficiency (e.g., as shown in Figure 4a, the intercalation contribution is lower on the 200th cycle as compared to the 100th cycle, but the CE of both cycles are the same at 99.6%).

At a higher lithiation capacity (2.0 mA h cm^{-2}) and current density (1.0 mA cm^{-2}), the Li plating/stripping process on planar Cu becomes even less efficient. As shown in Figure 3(b), the CE fluctuates from the beginning and only reaches 98% for a few cycles. It then becomes unstable after 25 cycles, whilst the average plateau overpotential abruptly drops to ca. −15 mV as shown in Figure S5(d), likely indicating a soft internal short-circuit caused by the sharp dendrites piercing through the separator.[59]

In contrast, the CFP electrode still performs satisfactorily under these strenuous electrochemical conditions, achieving a CE of ca. 99.5%, which only drops to 99% at the 150th cycle as shown in Figure 3(b). The high stability of the combined

Batteries & Supercaps

Research Article
doi.org/10.1002/batt.202100399

Chemistry Europe
European Chemical
Societies Publishing

intercalation and plating process is further illustrated by the highly repeatable voltage profiles of the 2nd, 50th, 100th and 150th cycles as shown in Figure S5(c). Furthermore, as shown in Figure 4(b), the nucleation overpotentials are consistently low at ca. −5 mV throughout the lifetime of the cell, despite the higher current density and lithiation capacity. As shown in Figure 4(c), the average plateau overpotentials are slightly higher than that of the CFP|Li cell tested at 0.5 mA cm^{-2} and 1.5 mA h cm^{-2}, but still stabilize at ca. −33 mV and show a generally decreasing trend.

Notably, lithiation/delithiation on CFP becomes much less efficient or repeatable when a conventional LiPF$_6$ in ethylene carbonate/ethyl methyl carbonate (EC/EMC) electrolyte is used (a stable CE of ca. 95% for 130 cycles and ca. 92% for 110 cycles under the respective electrochemical conditions as shown in Figure 3a and b). This shows the importance of LiNO$_3$ additive (with LiTFSI salt in DOL/DME solvent mix) to the performance of CFP electrodes and other LMA systems.[24] The reduction of LiNO$_3$ on Li helps to form a thin and stable SEI layer containing inorganic Li$_x$NO$_y$ species, which suppresses Li dendrite growth.[21,63]

A closer investigation of the electrochemistry of the CFP electrode after the 150th cycle reveals more information regarding its possible failure mechanism. As shown in Figure 3(b), the CE drops 0.4% between the 130th and 150th cycle to 99%, and a further 1.7% between the 150th and 170th cycle. As shown in Figure 4(c and d), the progressively faster CE decline is correlated with a quicker decay of the intercalation contribution, which sees a deviation from the originally linear trend from around the 130th cycle, as well as an increase in the plateau overpotential. This suggests that the decay of the CE after the 130th cycle is ultimately caused by the efficiency reduction of the Li plating/stripping contribution. Increasingly more Li metal are left unretrieved around the carbon fibers each cycle, which simultaneously prevents intercalated Li from diffusing out, and reduces the intercalation contribution of the next cycle, leading to even more Li being deposited by plating (now less efficient) and thus aggravating the overall CE degradation. The increasing amounts of porous and electronically isolated Li islands also add more resistance to the Li-ion transfer, which lead to the higher plateau overpotentials. Figure S6(d) shows the morphology of a fully-stripped CFP electrode after 210 cycles (last 30 cycles with CEs of below 98% and accelerated decay of the intercalation contributions as shown in Figure S6a–c) at a lithiation capacity of 2.0 mA h cm^{-2} and current density of 0.5 mA cm^{-2}. The pores of the carbon fiber network are now filled up with electronically isolated Li deposits and (likely to be) excess SEI buildup, making the fibers undistinguishable. The sudden drop of the Li plating/stripping regime efficiency is likely caused by the combined effect of the gradual build-up of residue Li and the continuous consumption of LiNO$_3$.[23,24,64] These deteriorations occur sooner when the lithiation capacity and/or current density is higher. As shown in Figure 4(d), at a lithiation capacity of 2.0 mA h cm^{-2} per cycle, the CFP electrode lasts 50 more cycles before the CE drops to 98% when the current density is halved from 1.0 mA cm^{-2} to 0.5 mA cm^{-2}. The cycle life is further improved by 90 cycles

when the lithiation capacity is reduced to 1.5 mA h cm^{-2} per cycle. The impact of higher current density is twofold: firstly, it increases polarization which leads to more Li plating/stripping contribution as the voltage drops to below 0 V before the full intercalation capacity is reached; secondly, it induces higher local current density which accelerates Li dendrite formation and growth according to Sand's Law.[27–29]

The CE, cycle life, and nucleation overpotentials achieved by these CFP electrodes are among the best reported for high capacity LMA 3D hosts.[49] The CFP electrode is especially advantageous because comparable technologies reported in literature often i) are tested with only 0.5–1.0 mA h cm^{-2} of lithiation capacity per cycle, which has been termed 'shallow' Li deposition/dissolution that artificially prolongs cycle life;[62] ii) do not discuss the Li consumption during a 'conditioning lithiation step' before the electrochemical tests whereby the working electrode is cycled at a low current density (such as 0.05 mA cm^{-2}) for a number of cycles to pre-form the SEI and artificially improve reported CEs; iii) have a very intricate manufacturing process that is difficult to scale up; iv) require an additional metal current collector which reduces the gravimetric and volumetric capacity.

Furthermore, as shown in Figure S3, a CFP|Li pouch cell (with no additional metal foil current collectors) shows similar CEs and voltage profiles as compared to the CFP|Li coin cell, when tested at a lithiation capacity of 1.5 mA h cm^{-2} and a current density of 0.5 mA cm^{-2}. This demonstrates that the highly-conductive CFP can be used as a freestanding electrode, which further improves the energy density of the battery system.

The CFP's capability as a Li host is further evaluated in a CFP-Li|CFP symmetric cell (Li is preloaded onto one CFP electrode), which unlike a half-cell is not affected by side reactions on the Li chip counter electrode. In contrast to the symmetric cell tests in most LMA studies whereby a reservoir of Li is kept on both electrodes and only a small proportion of the available Li is being cycled,[49] the two CFP electrodes in this study are fully delithiated (up to 1 V/−1 V) on every cycle. As shown in Figure 5(a), at a current density of 0.5 mA cm^{-2}, the CE of the CFP-Li|CFP cell stabilizes at ca. 99.6% for 30 cycles, before increasing to above 99.8% on the 50th cycle and maintaining this value for more than 400 cycles. As shown in Figure 5(c), more than 50% of the cell capacity is retained after 200 cycles and the capacity decay becomes increasingly slower.

Conclusion

In summary, a freestanding graphitized carbon fiber paper with carbon fillers is successfully demonstrated as an anode with a dual energy storage mechanism: First acts as a host for Li intercalation and then provides a 3D scaffold for efficient Li plating/stripping. In these electrodes, the 3D plating scaffold, which is essentially dead weight in classic LMAs, is turned into an active material contributing to energy storage. The Li-intercalated graphitic carbons have high lithiophilicity, which helps to reduce the energy barrier for Li nucleation, whilst the
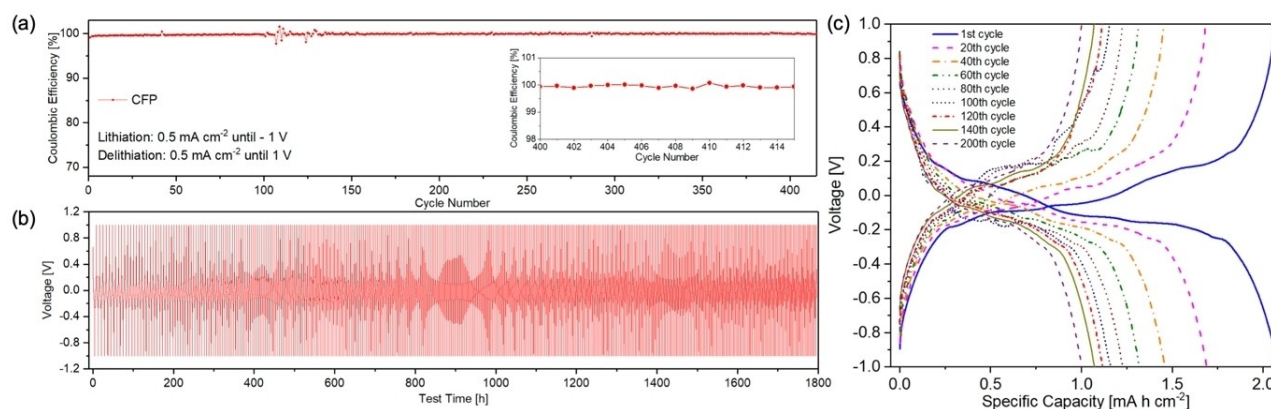
Batteries & Supercaps

Research Article
doi.org/10.1002/batt.202100399

Chemistry Europe
European Chemical
Societies Publishing

Figure 5. a) Coulombic efficiencies of a CFP-Li│CFP symmetric cell at a current density of 0.5 mA cm^{-2}. Inset shows the expanded view of CE between cycle 400 and 415. b) Voltage time profiles of all cycles. c) Voltage vs specific capacity profiles of the 1st, 20th, 40th, 60th, 80th, 100th, 120th, 140th and 200th cycles.

porous and conductive architecture offers abundant and well-distributed sites for Li nucleation. As a result, the CFP electrode demonstrates excellent cycling efficiency and stability, achieving Coulombic efficiencies of over 99.5% on the 250th cycle and 99% on the 300th cycle, and nucleation overpotentials of only ca. −5 to −6 mV in CFP│Li half-cells, with a lithiation capacity of 1.5 mA h cm^{-2} and current density of 0.5 mA cm^{-2}. Moreover, CFP can be manufactured cost-effectively at large scale, operate as a freestanding electrode without needing a metal current collector, and do not require additional surface coating, therefore showing potential for practical applications.

Experimental

Preparation of electrodes: A commercial CFP electrode (SIGRACET® GDL 39 AA gas diffusion layer from SGL Carbon SE) was cut into 15 mm ∅ circular disks (for half-cell and symmetric cell tests), 10 mm ∅ circular disks (optical cell tests) or 20 mm × 19 mm rectangles (pouch cell tests). For comparison, 8 μm thick planar Cu electrodes (MTI Corporation) were cut into 15 mm ∅ circular disks. The CFP and Cu electrodes were dried in a vacuum oven at 120 °C overnight before cell assembly. Li foil (MTI Corporation) was punched into 14 mm ∅ circular disks (half-cell and symmetric cell tests), 9 mm ∅ circular disks (optical cell tests) or 18 mm × 17 mm rectangles (pouch cell tests) in an argon-filled glove box.

Electrochemical measurements: CR2032 (MTI Corporation) type coin cells were assembled in an argon-filled glovebox ($O_2 <$ 0.5 ppm, $H_2O < 0.5$ ppm) to test the electrochemical performance of the CFP electrodes. 1.0 M LiTFSI in 1,3-dioxolane/1,2-dimethoxyethane (DOL/DME) (1:1 by volume) electrolyte with 3 wt.% LiNO$_3$ additive and Celgard 2500 separators were used in all tests (coin cells, optical cells and pouch cells), unless otherwise specified. For half-cell tests, freestanding CFP (no Cu current collector) was used as the working electrode and Li foil as the counter electrode. In the first cycle, the working electrode was formed at a low current density of 0.1 mA cm^{-2} until the cell reached 0 V, then 1.5–3 mA h cm^{-2} of capacity was deposited at 0.5–1 mA cm^{-2}. Next, Li was stripped from the working electrode at the same current density until the cell reached 1 V. Subsequent cycles were carried out at the testing current density (0.5–1 mA cm^{-2}). To verify the CFP's performance as a Li intercalation host only (no Li plating/stripping), half-cells were cycled between 1 V and 20 mV at a current density of 0.5 mA cm^{-2}. For symmetric cell tests, CFP-Li

electrodes were firstly prepared in the above half-cell configuration by depositing 3 mA h cm^{-2} of capacity at a current density of 0.5 mA cm^{-2}. The CFP-Li electrodes were then removed from the cells in a glovebox and placed in new coin cells with pristine CFP electrodes. After a formation cycle for the pristine CFP electrode, the CFP-Li│CFP cell was cycled between 1 V and −1 V at a current density of 0.5 mA cm^{-2}. Optical cells were built using an ECC-Opto-Std (EL-CELL) system with a 10 mm ∅ glass window. EL-CELL glass-fiber separators were used. A copper mesh current collector was added between the separator and the CFP electrode to connect the electrode contact pin and the electrode. To demonstrate CFP's capability as a freestanding electrode without a current collector (such as Cu foil), pouch cells were constructed using CFP as the working electrode and a Li chip as counter electrode, with aluminum laminated film (MTI) pouch cell casings and nickel tabs (MTI) as electrode terminals, as shown in Figure S2(a). All cells were rested for at least 24 h after assembly for the electrodes to be fully wetted by the electrolyte before measurements were carried out. The electrochemical data was recorded using a LAND (Wuhan LANHE Inc.) or VMP3 (Biologic) battery test system in a climate chamber at 25 °C.

Material characterizations: The morphologies of CFP at different lithiation stages were characterized in-situ by taking microscopic images of the electrodes through an optical cell using an Olympus BX53M microscope (20×lens) with an Olympus LC30 camera. Ex-situ images of CFP electrodes after cycling in coin-cells were taken by firstly dissembling the coin-cell, then moving the electrode to an optical cell. SEM images of the CFP were taken using a Leo variable pressure scanning electron microscope (SEM) at 5 kV with an in-lens secondary electron detector. XRD patterns of the electrodes were collected using a Philips/Panalytical PW3050/65 X'Pert PRO HR horizontal diffractometer with Cu K_α radiation ($\lambda =$ 1.5406 Å). Thermogravimetric analysis (TGA) of the CFP was carried out using a Perkin Elmer Pyris I system, at a heating rate of 5 °C min^{-1} from 30 °C to 800 °C under synthetic air with a flow rate of 20 mL min^{-1}.

Author Contributions

The manuscript was written through contributions of all authors. All authors have given approval to the final version of the manuscript.

Conflict of Interest

The authors declare no conflict of interest.

Data Availability Statement

The data that support the findings of this study are available from the corresponding author upon reasonable request.

[1] J. M. Tarascon, M. Armand, *Nature* **2001**, *414*, 359–367.
[2] N. Nitta, F. Wu, J. T. Lee, G. Yushin, *Mater. Today* **2015**, *18*, 252.
[3] J. Janek, W. G. Zeier, *Nat. Energy* **2016**, *1*, 1–4.
[4] A. C. Luntz, J. Voss, K. Reuter, *J. Phys. Chem. Lett.* **2015**, *6*, 4599–4604.
[5] Y. Yamada, K. Usui, C. H. Chiang, K. Kikuchi, K. Furukawa, A. Yamada, *ACS Appl. Mater. Interfaces* **2014**, *6*, 10892–10899.
[6] D. Lin, Y. Liu, Y. Cui, *Nat. Nanotechnol.* **2017**, *12*, 194–206.
[7] W. Xu, J. Wang, F. Ding, X. Chen, E. Nasybulin, Y. Zhang, J. G. Zhang, *Energy Environ. Sci.* **2014**, *7*, 513–537.
[8] Y. Sun, N. Liu, Y. Cui, *Nat. Energy* **2016**, *1*, 1–12.
[9] P. Y. Zhai, H. J. Peng, X. B. Cheng, L. Zhu, J. Q. Huang, W. Zhu, Q. Zhang, *Energy Storage Mater.* **2017**, *7*, 56.
[10] H. J. Peng, D. W. Wang, J. Q. Huang, X. B. Cheng, Z. Yuan, F. Wei, Q. Zhang, *Adv. Sci.* **2015**, *3*, 1500268.
[11] X.-B. Cheng, R. Zhang, C.-Z. Zhao, Q. Zhang, *Chem. Rev.* **2017**, *117*, 10403.
[12] A. Mukhopadhyay, M. K. Jangid, *Science* **2018**, *359*, 1463.
[13] R. Schweiss, C. Meiser, T. Damjanovic, I. Galbiati, N. Haak, *SGL Gr.* **2016**, 1.
[14] W. Go, M. H. Kim, J. Park, C. H. Lim, S. H. Joo, Y. Kim, H. W. Lee, *Nano Lett.* **2019**, *19*, 1504.
[15] L. Cheng, L. A. Curtiss, K. R. Zavadil, A. A. Gewirth, Y. Shao, K. G. Gallagher, *ACS Energy Lett.* **2016**, *1*, 503–509.
[16] K. Xu, *Chem. Rev.* **2004**, *104*, 4303.
[17] R. Miao, J. Yang, X. Feng, H. Jia, J. Wang, Y. Nuli, *J. Power Sources* **2014**, *271*, 291.
[18] F. Qiu, X. Li, H. Deng, D. Wang, X. Mu, P. He, H. Zhou, *Adv. Energy Mater.* **2019**, *9*, 1803372.
[19] J. Zheng, M. H. Engelhard, D. Mei, S. Jiao, B. J. Polzin, J. G. Zhang, W. Xu, *Nat. Energy* **2017**, *2*, 17012.
[20] A. Jozwiuk, B. B. Berkes, T. Weiß, H. Sommer, J. Janek, T. Brezesinski, *Energy Environ. Sci.* **2016**, *9*, 2603.
[21] A. Rosenman, R. Elazari, G. Salitra, E. Markevich, D. Aurbach, A. Garsuch, *J. Electrochem. Soc.* **2015**, *162*, A470.
[22] B. D. Adams, E. V. Carino, J. G. Connell, K. S. Han, R. Cao, J. Chen, J. Zheng, Q. Li, K. T. Mueller, W. A. Henderson, J. G. Zhang, *Nano Energy* **2017**, *40*, 607.
[23] S. Xiong, K. Xie, Y. Diao, X. Hong, *Electrochim. Acta* **2012**, *83*, 78.
[24] S. S. Zhang, *Electrochim. Acta* **2012**, *70*, 344.
[25] J. Scheers, S. Fantini, P. Johansson, *J. Power Sources* **2014**, *255*, 204.
[26] A. Manthiram, Y. Fu, S. H. Chung, C. Zu, Y. S. Su, *Chem. Rev.* **2014**, *114*, 11751–11787.
[27] C. Brissot, M. Rosso, J. N. Chazalviel, S. Lascaud, *J. Power Sources* **1999**, *81*, 925.
[28] M. Rosso, C. Brissot, A. Teyssot, M. Dollé, L. Sannier, J. M. Tarascon, R. Bouchet, S. Lascaud, *Electrochim. Acta* **2006**, *51*, 5334.
[29] K. Nishikawa, T. Mori, T. Nishida, Y. Fukunaka, M. Rosso, *J. Electroanal. Chem.* **2011**, *661*, 84.
[30] Y. Son, T. Lee, B. Wen, J. Ma, C. Jo, Y.-G. Cho, A. Boies, J. Cho, M. De Volder, *Energy Environ. Sci.* **2020**, *13*, 3723.
[31] X. B. Cheng, H. J. Peng, J. Q. Huang, R. Zhang, C. Z. Zhao, Q. Zhang, *ACS Nano* **2015**, *9*, 6373.
[32] R. Zhang, X. B. Cheng, C. Z. Zhao, H. J. Peng, J. Le Shi, J. Q. Huang, J. Wang, F. Wei, Q. Zhang, *Adv. Mater.* **2016**, *28*, 2155.
[33] R. Mukherjee, A. V. Thomas, D. Datta, E. Singh, J. Li, O. Eksik, V. B. Shenoy, N. Koratkar, *Nat. Commun.* **2014**, *5*, 3710.
[34] G. Zheng, S. W. Lee, Z. Liang, H.-W. Lee, K. Yan, H. Yao, H. Wang, W. Li, S. Chu, Y. Cui, *Nat. Nanotechnol.* **2014**, *9*, 618.
[35] H. Ye, S. Xin, Y. X. Yin, J. Y. Li, Y. G. Guo, L. J. Wan, *J. Am. Chem. Soc.* **2017**, *139*, 5916.
[36] S. Matsuda, Y. Kubo, K. Uosaki, S. Nakanishi, *Carbon* **2017**, *119*, 119.
[37] Z. Sun, S. Jin, H. Jin, Z. Du, Y. Zhu, A. Cao, H. Ji, L. J. Wan, *Adv. Mater.* **2018**, *30*, 1.
[38] A. R. O. Raji, R. Villegas Salvatierra, N. D. Kim, X. Fan, Y. Li, G. A. L. Silva, J. Sha, J. M. Tour, *ACS Nano* **2017**, *11*, 6362.
[39] Y. Zhang, B. Liu, E. Hitz, W. Luo, Y. Yao, Y. Li, J. Dai, C. Chen, Y. Wang, C. Yang, H. Li, L. Hu, *Nano Res.* **2017**, *10*, 1356.
[40] A. Zhang, X. Fang, C. Shen, Y. Liu, C. Zhou, *Nano Res.* **2016**, *9*, 3428.
[41] Z. J. Fan, J. Yan, T. Wei, G. Q. Ning, L. J. Zhi, J. C. Liu, D. X. Cao, G. L. Wang, F. Wei, *ACS Nano* **2011**, *5*, 2787.
[42] Z. Li, B. Tang, *Green Chem.* **2017**, *19*, 5862.
[43] L. Zhang, S. Peng, Y. Ding, X. Guo, Y. Qian, H. Celio, G. He, G. Yu, *Energy Environ. Sci.* **2019**, *12*, 1989.
[44] M. Akia, N. Salinas, S. Luna, E. Medina, A. Valdez, J. Lopez, J. Ayala, M. Alcoutlabi, K. Lozano, *J. Mater. Sci.* **2019**, *54*, 13479.
[45] Y. Du, C. Liu, Y. Liu, Q. Han, X. Chi, Y. Liu, *Electrochim. Acta* **2020**, *339*, 135867.
[46] X. Ji, D. Y. Liu, D. G. Prendiville, Y. Zhang, X. Liu, G. D. Stucky, *Nano Today* **2012**, *7*, 10.
[47] C. Niu, H. Pan, W. Xu, J. Xiao, J.-G. Zhang, L. Luo, C. Wang, D. Mei, J. Meng, X. Wang, Z. Liu, L. Mai, J. Liu, *Nat. Nanotechnol.* **2019**, 1.
[48] L. Liu, Y. X. Yin, J. Y. Li, S. H. Wang, Y. G. Guo, L. J. Wan, *Adv. Mater.* **2018**, *30*, 1.
[49] S. Park, H. J. Jin, Y. S. Yun, *Adv. Mater.* **2020**, *2002193*, 1.
[50] T. Chen, W. Jia, Z. Yao, Y. Liu, X. Guan, K. Li, J. Xiao, H. Liu, Y. Chen, Y. Zhou, D. Sun, J. Li, *Electrochem. Commun.* **2019**, *107*, 106535.
[51] T. T. Zuo, X. W. Wu, C. P. Yang, Y. X. Yin, H. Ye, N. W. Li, Y. G. Guo, *Adv. Mater.* **2017**, *29*, 1.
[52] S. Hasanpour, M. Hoorfar, A. B. Phillion, *J. Power Sources* **2017**, *353*, 221.
[53] J. P. Feser, A. K. Prasad, S. G. Advani, *J. Power Sources* **2006**, *162*, 1226.
[54] A. Lamibrac, J. Roth, M. Toulec, F. Marone, M. Stampanoni, F. N. Büchi, *J. Electrochem. Soc.* **2016**, *163*, F202.
[55] D. Bom, R. Andrews, D. Jacques, J. Anthony, B. Chen, M. S. Meier, J. P. Selegue, *Nano Lett.* **2002**, *2*, 615.
[56] M. Drüe, M. Seyring, M. Rettenmayr, *J. Power Sources* **2017**, *353*, 58.
[57] M. Inaba, *J. Electrochem. Soc.* **1995**, *142*, 20.
[58] T. Ohzuku, *J. Electrochem. Soc.* **1993**, *140*, 2490.
[59] Q. Li, S. Zhu, Y. Lu, *Adv. Funct. Mater.* **2017**, *27*, 1.
[60] K. Yan, Z. Lu, H. W. Lee, F. Xiong, P. C. Hsu, Y. Li, J. Zhao, S. Chu, Y. Cui, *Nat. Energy* **2016**, *1*, 16010.
[61] A. Pei, G. Zheng, F. Shi, Y. Li, Y. Cui, *Nano Lett.* **2017**, *17*, 45.
[62] J. Liu, Z. Bao, Y. Cui, E. J. Dufek, J. B. Goodenough, P. Khalifah, Q. Li, B. Y. Liaw, P. Liu, A. Manthiram, Y. S. Meng, V. R. Subramanian, M. F. Toney, V. V. Viswanathan, M. S. Whittingham, J. Xiao, W. Xu, J. Yang, X. Q. Yang, J. G. Zhang, *Nat. Energy* **2019**, *4*, 180–186.
[63] S. Xiong, K. Xie, Y. Diao, X. Hong, *Electrochim. Acta* **2012**, *83*, 78.
[64] M. Agostini, M. Sadd, S. Xiong, C. Cavallo, J. Heo, J. H. Ahn, A. Matic, *ChemSusChem* **2019**, *12*, 4176.